Int. J. Electrochem. Sci., 16 **(2021)** Article ID: 210931, doi: 10.20964/2021.09.42

International Journal of
ELECTROCHEMICAL
SCIENCE
www.electrochemsci.org

One-step Electrochemical Synthesis of Free-Standing Cobalt Oxide Nanoflakes to Fabricate Amperometric Sensor for the Acetaminophen Detection in Human Fluids and Pharmaceutical Formulations

Zong-Mu Dong[*], *Tong Sun, Peiyi Zhang, Miao-Qin Xu, Guang-Chao Zhao*

School of Ecology and Environment, Anhui Normal University, Wuhu 241002, P.R China
[*]E-mail: dzongmu@mail.ahnu.edu.cn

Received: 1 June 2021 / *Accepted:* 13 July 2021 / *Published:* 10 August 2021

Free-standing cobalt oxide nanoflakes were synthetized directly on a glassy carbon electrode via an one-step electrodeposition. A stable and sensitive amperometric sensor based on the cobalt oxide nanoflakes was developed for the acetaminophen detection, with a high sensitivity of 5042 $\mu A \cdot mM^{-1} \cdot cm^{-2}$, and a detection limit of 0.015 μM at the applied potential of 0.47 V. The high sensitivity and stability towards acetaminophen detection are mainly attributed to direct electrochemical growth and self-supported features of the cobalt oxide nanoflakes on a conducting substrate. The sensor was successfully applied for the determination of acetaminophen in serum, urine samples and commercial tablets.

Keywords: cobalt oxide nanoflakes, acetaminophen, sensor, electrochemical synthesis

1. INTRODUCTION

As an anti-infective drug, acetaminophen (AAP) is one of the members of the nonsteroidal analgesic and antipyretic medicaments families, which are most extensively used by patients in the world [1, 2]. Clinically, it is usually a painkiller and antipyretic drug against influenza and that is mainly used to treat ailments including arthralgia, neuralgia, migraine, back pain, arthritis and postoperative pain. It still can be detected in urine, although the entire AAP at normal doses can be quickly metabolized to inactive metabolites by the glucuronidation and sulfation in the body [3, 4]. However, the large consumption amount of AAP (up to 4.0 g/day) or over a long period of time can cause dangerous to human health even death for adults. In another way, despite the AAP as a prescription drug is strictly limited in the safe use of doses, it leads to damage kidney and liver due to interaction with alcohol [5, 6]. Hence, concerning the health effects from the overdose of AAP as mentioned earlier, the

concentration of AAP in pharmaceutical formulations should be controlled and it is highly essential to determine the AAP accurately from pharma as well as the human fluids (plasma and urine, etc.) after consumption.

Until now several techniques have been reported for the quantification of AAP in human fluids and pharmaceutical preparations such as HPLC [7], LC-MS [8], GC-MS [9], UV-spectrofluorometry [10], chemiluminescence [11], capillary electrophoresis [12]， and FT-IR spectrophotometric analysis [13]. However, these methods hare several limitations such as relatively expensive, long time working analysis, need for pre-sample preparation and have multi-step sample processing procedures. In general, the electrochemical method is an alternative among many analytical methods, which is quick response results (timesaving), economically viable, portable (more efficient), higher sensitivity, excellent selectivity and good practicability for the accurate determination of AAP [14-20]. Moreover, electrochemical sensing devices and nano-catalytic material modified electrodes have been widely used in vast of areas including environmental analysis, biological sensors, molecular biology, food and pharmaceutical drug analysis, agricultural inspections.

The selection of catalysts with excellent performance and the simple and convenient construction of electrochemical sensors are crucial factors for the accurate quantification of AAP. In the past decades, cobalt oxide-related nanostructures have increasingly been utilized for construction of electrochemical sensors because of its surprising properties resulting from the nanoscale characteristics and catalytic activity for many biomolecules. The cobalt oxide has three well-known polymorphs: the cobaltous oxide (CoO), the cobaltic oxide (Co_2O_3) and the cobaltosic oxide (Co_3O_4), which make it a photochemical and electrochemical electrode material with excellent catalytic properties [21]. Many methods have been developed to prepare cobalt oxide nanoparticles, including sol-gel [22], chemical vapor deposition [23], electrophoretic deposition [24] and chemical precursor routes [25, 26]. Furthermore, many researches have been reported for fabricating metal oxides-based sensors, which mainly included two procedures. One is a multistep synthesizing the metal oxides nanoparticles obtained. Another is to attach the as-prepared metal oxides nanoparticles on an electrode support material for example the electrochemically reduced graphene oxide (rGO) [18], aminotriazzine (AT) [14], Nafion (Nf) [17], graphene augmented inorganic nanofibers (GAIN) [19], multi-walled carbon nanotubes (MWCNTs) [27], carbon spherical shells (CSS) [28], poly(3,4-ethylenedioxythiophene) nanotubes (PEDOT NT) [29], and composite metal nanoparticles [30] etc. However, most of these synthesis methods were complicated for the electrode materials, and with multistep reaction process for the electrode modification. The application of various agents would leave many chemical residues, which are not environmentally friendly.

In this work, a facile electrodeposited strategy was employed to synthesize free-standing Co_3O_4 nanoflakes (Co_3O_4 NFs) onto a glass carbon electrode (Co_3O_4 NFs /GCE), and one-step fabricate electrochemical sensor for AAP detection. Compared with other fabricating metal oxides-based sensors, our method for the preparation of Co_3O_4 nanoflakes-based sensor has several advantages such as one-step fabrication and avoid a multistep electrode modifying process, flexible control, high stability and a simple, effective operation. The transmission electron microscopy (TEM), X-ray diffraction (XRD), electrochemical quartz crystal microbalance (EQCM) and cyclic voltammetry (CV) techniques were used to characterize the structure and performances of Co_3O_4 nanoflakes, which indicated that free-standing Co_3O_4 nanoflakes were successfully synthesized with high catalytic ability as well as good

conductivity. The Co_3O_4 NFs/GCE exhibited substantial electrocatalytic activity and superior analytical performance towards the AAP, which also showed lowest detection limit and excellent sensitivity besides the storage capability, well repeatability and reproducibility. Furthermore, the Co_3O_4 NFs /GCE was used for the quantification of the AAP in human biofluids and pharmaceutical formulations.

2. EXPERIMENTAL

2.1 Reagents

Cobalt chloride hexahydrate ($CoCl_2 \cdot 6H_2O$) and sodium hydroxide (NaOH, pellets) were purchased from Shanghai Chemical Corp (http://www. reagent.com.cn). Ascorbic acid, uric acid, glucose, human serum and acetaminophen were obtained from Sigma-Aldrich (http: //www. sigmaaldrich.com). Phosphate buffer solution (PBS, pH, 7.4) was prepared by mixing $Na_2HPO_4 \cdot 2H_2O$ and NaH_2PO_4 in deionized water. All aqueous solutions were prepared with deionized water (18.6 MΩ cm^{-2}) generated by a Milli-Q water system.

2.2 Preparation of Co_3O_4 NFs/GCE

Prior to surface electrodeposition, glass carbon electrode (GCE, diameter 3 mm) was polished with 0.03 μm alumina slurries, and then rinsed with deionized water. Films of cobalt oxide were deposited cathodically by potentiostatic condition at -1.0 V (vs. Ag/AgCl). The deposition was performed in deaerated 10 mM $CoCl_2$ solution containing 0.1 M HCl. The amount of cobalt on the surface of the electrode was regulated by the electrodeposition time and EQCM measurements. Subsequently, the electrode was performed in 0.1 M PBS under the regime of cyclic voltammetry where consecutive cycles (more than 10 times) in the range of -0.2 to 0.8 V with a potential sweep rate of 0.1 V s^{-1} were applied until a steady cyclic voltammogram was observed.

2.3 Apparatus and electrochemical measurements

SEM images were obtained on a Hitachi S-4800 field emission scanning electron microscope operated at an accelerating voltage of 5.0 kV. The X-ray powder diffraction (XRD) analysis of the product was carried out on a Shimadzu XRD-6000 X-ray diffractometer, employing a scanning rate of 0.02° s^{-1}. EQCM measurements were performed on a quartz crystal microbalance (CHI 440 A, CH Instruments, Inc. USA). All electrochemical experiments were carried with an Epsilon MF-9092 electrochemical workstation (Bioanalytical Systems, Inc. USA) with a conventional three-electrode cell. An as-prepared Co_3O_4 NFs/GCE, Ag/AgCl electrode, and platinum wire electrode served as the working electrode, reference electrode, and counter electrode, respectively. All the potential values in this paper refer to the Ag/AgCl reference electrode.

3. RESULTS AND DISCUSSION

3.1 Characterization of Co_3O_4 NFs

SEM was used to investigate the morphology and microstructure of Co_3O_4 NFs. As shown in Fig. 1, the flake-liked crystalline morphology of Co_3O_4 was well presented (Fig. 1A). The thickness of the nanoflake was in the range of 5-10 nm. Moreover, it was found that some nanoparticles tended to aggregate and exhibited anisotropic growth, and a lot of flower-like structures were observed (Fig. 1B) with deposition time increased (30 s). The amount of Co_3O_4 NFs electrodeposition was measured by EQCM, as shown in Fig. 1D. According to the Sauerbrey equation [31], $\Delta f = -C_f \times \Delta m$, the response value of EQCM within 30 seconds was 359 Hz, indicating that the amount of Co_3O_4 NFs deposition on the electrode was 2528.16 ng cm^{-1}. As shown in the frequency response curve in the red elliptical circle in Fig. 1D, when the electrolysis stopped, the frequency of EQCM did not change, indicating that the Co_3O_4 NFs was no longer formed.

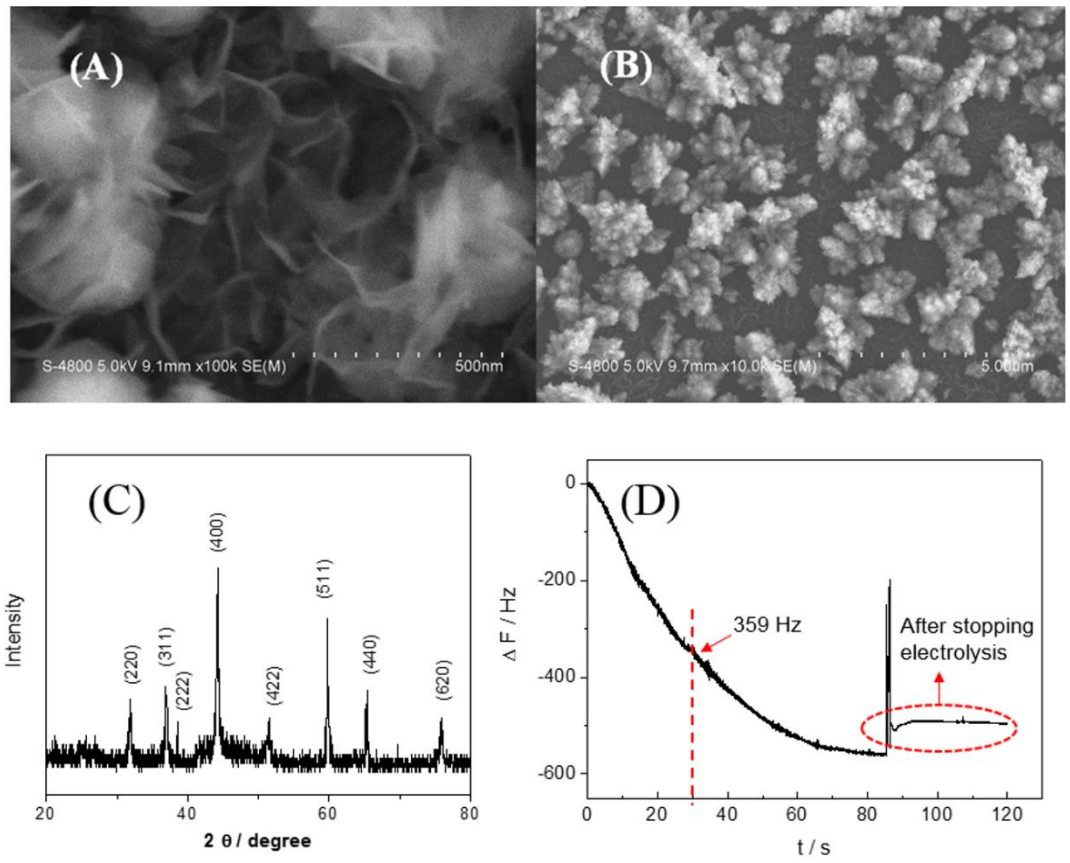

Figure 1. SEM images of Co_3O_4 NFs on the GCE substrate. (A) high-magnification, (B) low-magnification. (C) XRD spectrum of Co_3O_4 nanoflakes. (D) EQCM response of Co_3O_4 electrodeposition, deposition potential -1.0 V vs. Ag/AgCl.

The crystal structure and phase purity of the as-prepared Co_3O_4 nanoflakes were further characterized by XRD. As shown in Fig. 1C, the XRD spectrum of Co_3O_4 nanoflakes matches the

standard spectrum of cubic crystalline Co_3O_4 (JCPDS 42-1467). The formation of cubic crystalline Co_3O_4 is revealed by the diffraction peaks at 2θ values of 31.3°, 36.8°, 38.5°, 44.8°, 56.7°, 59.4°, 65.2°, 74.1° corresponding to (220), (331), (222), (440), (422), (511), (440), and (620) crystal planes, respectively. No other impurities could be detected in the XRD pattern of Co_3O_4, indicating that Co_3O_4 was obtained [21]. These results showed Co_3O_4 nanoflakes had a large specific surface area that was promising to be excellent electrode materials.

3.2 Electrochemical behavior of the Co_3O_4 NFs/GCE

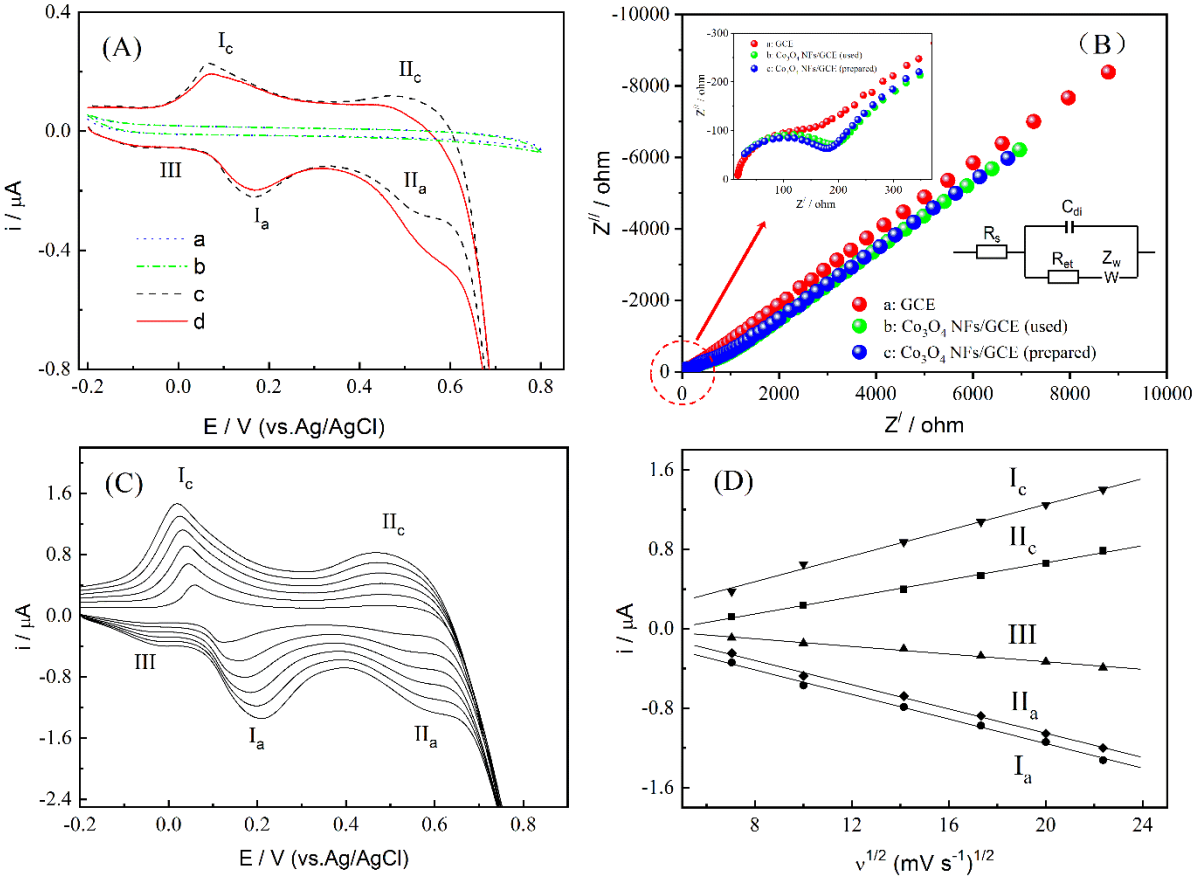

Figure 2. (A) CVs of the GCE (a and b) and Co_3O_4 NFs/GCE (c and d) in 0.1 M PB solution in the absence (a and c) and presence (b and d) of 0.01 mM AAP, respectively. (B) EIS responses of (a) GCE and Co_3O_4 NFs/GCE before (c, freshly prepared) and after (b, used) the detection of AAP in 0.1 M KCl / 1 mM $K_3[Fe(CN)_6]$ mixture at ±5 mV amplitude and 0.001 Hz to 10 kHz frequency. (Upper left inset: 1 Hz to 400 Hz frequency; Lower right inset: Randel's equivalent circuit). (C) CVs of the Co_3O_4 NFs/GCE in 0.1 M PB solution at various rates of 50, 100, 200, 300, 400, 500 mV/s; (D) Plot of peak current vs. one half power of the scan rates.

The cyclic voltammograms of the bare GCE and Co_3O_4 NFs/GCE were investigated in 0.1 M PB solution (pH, 7.4) in the range from -0.2 to 0.8 V (vs. Ag/AgCl). As shown in Fig 2A (a, b), no obvious oxidation or reduction peak of the bare GCE was observed in the absence and presence of AAP solution.

However, the pair of redox peaks I_a/I_c of Co_3O_4 NFs/GCE in 0.1 M PB solution can be assigned to the reversible oxidation-reduction reaction between Co_3O_4 and CoOOH, while another pair of redox peaks II_a/II_c can be attributed to further redox process between CoOOH and CoO_2 species (curve c of the Fig 2A) [32]. The anodic peak at approximately 0.0 V, III_a, could be an oxidation process of the hydroxyl ions, H_2OOH^-, adsorbed on the cobalt oxide film during cycling of the potentials in weakly alkaline medium [33].

The electronic conductivity of the Co_3O_4 NFs fabricated GCE were elucidated by the electrical impedance spectral studies. Fig. 2B displays the Nyquist plots of GCE and Co_3O_4 NFs/GCE. The Nyquist plot exhibited the linear portions at lower frequencies, which are associated with the diffusion behavior of electroactive species. Furthermore, the semicircle portions at higher frequencies (upper left inset in Fig. 2B), which are associated with the electrochemical process subject to electron transfer, and the diameter is resembled to the charge transfer resistance (R_{et}) of the electrode [34, 35]. The EIS data were fitted with the Randles equivalent circuit model (lower right inset in Fig. 2B). The bare GCE exhibited a smaller semicircle portion (curve a), revealing the lower R_{et} of 187 Ω and the excellent electrochemical diffusion process. The R_{et} value was increased slightly after fabricating the electrode with Co_3O_4 NFs, and it was found to be 206 Ω (curve c). Moreover, after the Co_3O_4 NFs/GCE has been used to detect AAP, its R_{et} value is 212 Ω, which is slightly higher than the R_{et} value before the test, indicating that the Co_3O_4 NFs/GCE was not contaminated by the electrode reaction intermediate during the application. The negligible increase in impedance indicates that both the prepared and used Co_3O_4 NFs/GCE retains excellent electron transfer properties between the electrode and electrolyte solution.

A family of cyclic voltammograms obtained with the electrodeposited Co_3O_4 NFs/GCE in 0.1 M PBS at the scan rates from 50 to 500 mV s^{-1} was shown in Fig. 2C. The dependence of peak current on one-half root of scan rate for peaks I_a, II_a, III, I_c, and II_c is shown in Fig. 2D. As can be seen, the peak currents of the waves were found to vary linearly with one-half root of scan rate up to 500 mV s^{-1}. Nevertheless, the peak potential of the peaks I_a, II_a, III, I_c, and II_c are practically independent of the scan rate. Thus, the overall redox process confined at the Co_3O_4 NFs/GCE surface can be considered relatively fast on voltametric time scale. Moreover, considering that the shapes of the waves are not perfectly symmetrical and the peak-to-peak separations of I_a/I_c and II_a/II_c redox transitions of the cobalt oxide species are under mixed control of both diffusion controlled and some kinetic limitations within the layer of the electroactive Co_3O_4 NFs film [36].

3.3 The voltammetric behavior and amperometric detection of acetaminophen at the Co_3O_4 NFs/GCE

The electrooxidation of AAP at the Co_3O_4 NFs/GCE was examined in 0.1 M PBS (pH, 7.4). Fig 2A presents the CVs in the absence and presence of 5.0 µM AAP, recorded at the GCE (curves a and c) and the Co_3O_4 NFs/GCE (curves b and d), respectively. An increased current response (peak II_a of the curve d in Fig. 2A) at Co_3O_4 NFs/GCE was observed in the present of 5 µM AAP covering the potential region between 0.25 V to 0.47 V. By contrast, no obvious response was found at GCE. Those results indicated that the Co_3O_4 NFs/GCE could retain high catalytic activity toward AAP oxidation in PBS. In addition, the current increase with the addition of AAP at the oxidation peak II_a was much stronger than

that at peak I, which may suggest that the electrooxidation of AAP is mainly mediated by $CoOOH/CoO_2$ rather than $CoO_4/CoOOH$ in 0.1 M PBS as shown in Fig.3B. Therefore, the peak II potential was applied for subsequent amperometric detection. The optimal value of the applied potential was obtained by amperometric measurement of AAP concentration in 0.1M PBS at different potentials as shown in Fig 3D. When the applied potential was increased from 0.25 to 0.47 V, the response current increased gradually. The maximum response current with a good signal/noise ratio was achieved at 0.47 V. The potential of 0.47 V was applied to perform amperometric detection of AAP in the weakly alkaline solution.

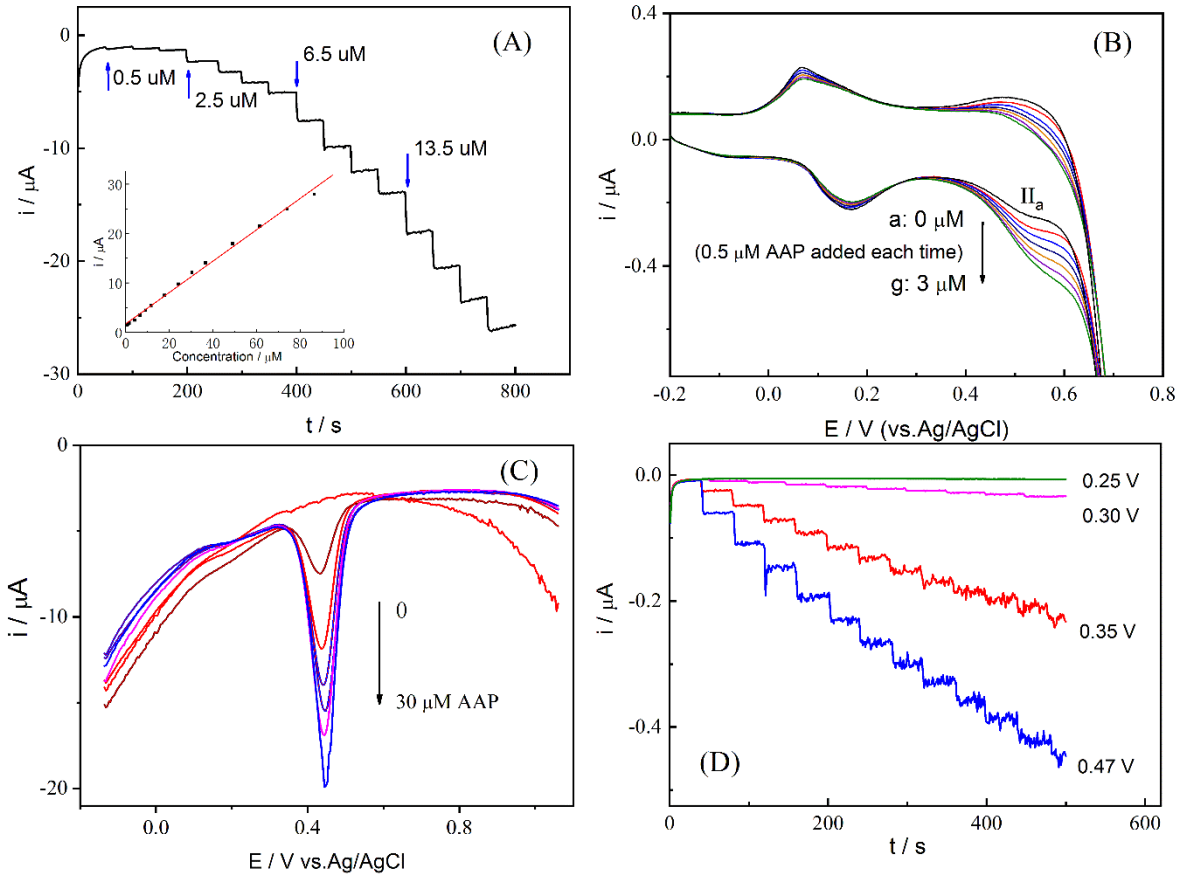

Figure 3. Amperometric (A) and CV (B) responses of the Co_3O_4 NFs/GCE AAP sensor for successive injection of vary concentration AAP in PBS (pH, 7.4). Inset of (A): calibration curves of AAP concentration at the Co_3O_4 NFs/GCE. (C) DPVs obtained for 0 − 40 μM addition of AAP (each 5 μM) at Co_3O_4 NFs/GCE in 0.1 M PB solution (pH, 7.4). (D) Dependence of the response currents on the applied potentials. In this experiment, 0.5 μM AAP was added each time.

Fig. 3A presented a typical amperometric response curve of AAP in 0.1 M PBS at the Co_3O_4 NFs/GCE. The current response of the electrode exhibited a linear region of AAP concentration. In 0.5-286.5 μM, the linear equation is y = 0.7410 + 0.0317 x (R = 0.9981), where y and x stand for the peak current (μA) and the concentration (μM) of AAP, respectively. The response time was less than 3 s with addition of 0.5 μM AAP and the limit of detection was 0.015 μM (S/N = 3). From the slope of the linear

portion of calibration curve and the working area of electrode, a high sensitivity of 5042 $\mu A \cdot mM^{-1} \cdot cm^{-2}$ was calculated for the Co_3O_4 NFs/GCE AAP sensor. In addition, the DPV responses of the Co_3O_4 NFs/GCE were shown in Fig. 3C (each 5 μM AAP added). The performances of Co_3O_4 NFs/GCE AAP sensor were compared with those of other published AAP sensors in Table 1. All the data from this sensor showed the properties of high sensitivity, low detection limit and fast response time. Therefore, the simple one-step electrodeposition of the Co_3O_4 nanoflakes and its good electrocatalytic ability make it an excellent sensor for AAP detection. Though the detection limit and sensitivity of the Co_3O_4 NFs/GCE sensor are not as good as the ERGO/AT/GCE based sensor [14], the Co_3O_4 nanoflakes electrodeposited offers important commercial advantages with lower cost.

Table 1. Comparison of AAP sensing performance based on different electrode materials.

Electrode	Method	Linear range(μM)	Detection limit (μM)	Sensitivity ($\mu A\ mM^{-1}\ cm^{-2}$)	Ref.
ERGO/AT/GCE	Amp	0.04-100	6.8×10^{-4}	-	[14]
Nf/GO-Ch Pd/GCE	Amp	0.04-800	1.2×10^{-2}	232.89	[17]
N-CeO_2@rGO/GCE	Amp	0.05-0.60	9.8×10^{-3}	268	[18]
GAIN/Cu/GCE	DPV	1.0-700	1.2×10^{-2}	-	[19]
Co/CS/f-MWCNTs/GCE	Amp	0.10-400	1.0×10^{-2}	-	[27]
CSS/GCE	DPV	0.37-7.52	0.12	20.0	[28]
rGO-PEDOT NT/GCE	Amp	1.0-35.0	0.40	16.85	[29]
Ag-P NPs/SPCE	DPV	1.0-1000	1.76×10^{-2}	1314.5	[30]
CS-CPE	SWV	0.80-1000	0.508	-	[37]
Co_3O_4 NFs/GCE	Amp	0.5-286.5	1.5×10^{-2}	5042	This work

Abbreviation comment： ERGO: Electrochemically reduced graphene oxide. AT: Aminotriazzine. GCE: Glassy carbon electrode. Nf: Nafion. GAIN: Graphene augmented inorganic nanofibers. CPE: Carbon paste electrode. CSS: Carbon spherical shells. PEDOT NT: Poly(3,4-ethylenedioxythiophene) nanotubes.

3.4 Selectivity, stability and reproducibility of the Co_3O_4 NFs/GCE

The selectivity of Co_3O_4 NFs/GCE was investigated against normally interfering species with AAP in real samples such as ascorbic acid (AA), glucose (Glu), uric acid (UA) and normal inorganic ions. Considering the concentration of AAP was at least 30 times of interfering species in human blood, the interference experiment was carried out by successive injection of 0.02 mM AAP, 0.1 mM glucose, 0.1 mM AA and 0.4 mM UA in 0.1 M PBS. As demonstrated in Fig.4A, 0.1 mM AA existed in 0.02 mM AAP solution can result in 16% increase of current response compared to the response for 0.02 mM AAP, while 0.4 mM UA, 0.1 mM Glu can only lead to 5% and 11% increase, respectively. Additional, the amperometric response of the Co_3O_4 NFs/GCE was tested in the presence and absence of 0.09 M

NaCl, 0.1 mM Mg^{2+} and 0.1 mM Ca^{2+} in 0.1 M PBS. The response at the Co_3O_4 NFs/GCE remains unchanged, implying that the Co_3O_4 NFs/GCE can work well for the sample with high concentration of chloride ions and normal metal ions.

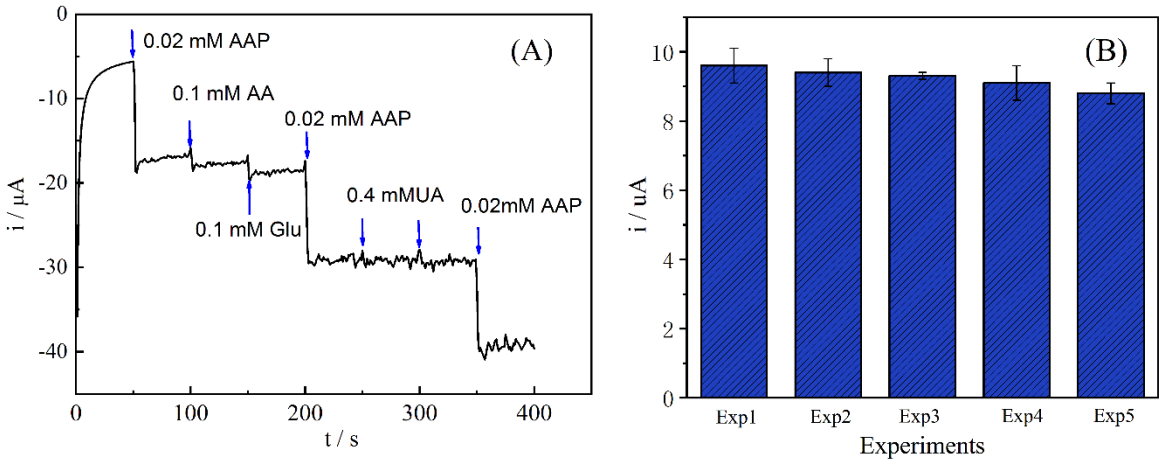

Figure 4. (A) Amperometric responses on the Co_3O_4 NFs/GCE sensor for successive injection of 0.02 mM AAP and interfering species (0.1 mM AA, 0.1 mM Glu and 0.4 mM UA) into 0.1 M PBS. (B) The amperometric current responses of five successive measurements of 25 μM AAP with one Co_3O_4 NFs/GCE at 0.47 V.

The reproducibility and stability of the Co_3O_4 nanoflakes sensor were evaluated. As be shown in Fig. 4B, five successive measurements of 25 μM AAP were performed with one Co_3O_4 NFs/GCE at 0.47 V to compare their amperometric current responses. The relative standard deviation (R.S.D) was 2.4%, indicating that the sensor had a satisfactory reproducibility. Furthermore, the stability of the Co_3O_4 NFs/GCE was also tested. As be shown in Fig.2B, after the Co_3O_4 NFs/GCE has been used to detect AAP, its R_{et} value of EIS is 212 Ω, which is slightly higher than the R_{et} value before the test, indicating that the Co_3O_4 NFs/GCE was not contaminated by the electrode reaction intermediate during the application. Both the freshly prepared and used Co_3O_4 NFs/GCE retains excellent electron transfer properties between the electrode and electrolyte solution. Moreover, when the Co_3O_4 NFs/GCE was stored at room temperature for two months, the current responses was approximately 96.8% of its original value. The results confirmed that the electrode could be used in long-term application. The excellent reproducibility and stability of the Co_3O_4 NFs/GCE could be attributed to the Co_3O_4 nanoflakes firmly linked with glass carbon electrode, good stability of the crystalline structure itself and good stability of the Co_3O_4 nanoflakes in the weakly alkaline solution.

3.5 Real sample analysis

In order to test the applicability of the developed free-standing Co_3O_4 NFs/GCE sensor, the human blood serum, urine samples were analysis by the standard addition method. The acetaminophen in commercial pills were directly quantified using the sensor. Prior to analysis, the blood serum sample

was diluted 10 times using PB solution (pH, 7.4). The detection results of blood serum samples were listed in table 2. The good recovery indicated that the Co_3O_4 NFs/GCE sensor could be effectively used for the AAP analysis in biological samples.

Table 2. Determination of AAP in diluted human blood serum, urine and commercial pharmaceutical formulations.

Sample	Added AAP (μM)	Found AAP (μM)	Recoveries (%)	R.S.D.% （n=5）
Serum sample	5.0	4.9	98.4	1.26
	10.0	9.9	98.9	0.79
	20.0	19.6	98.0	0.97
	50.0	49.2	98.4	1.19
	100.0	99.6	99.6	0.58
Urine sample	5.0	4.9	97.8	0.83
	10.0	9.7	97.0	0.68
	20.0	18.9	94.5	1.22
	50.0	49.6	99.2	0.93
	100.0	98.9	98.9	0.56
Pharmaceutical formulations	10.0	9.9	99.2	0.76
	20.0	20.3	101.5	0.98
	50.0	49.4	98.8	0.87
	100.0	98.6	98.6	1.31
	200.0	201.3	100.6	0.58

4. CONCLUSIONS

The process of one-step electrodeposited free-standing Co_3O_4 nanoflakes was simple without using complex synthesis and multistep modification of electrode materials. The Co_3O_4 NFs/GCE was easily fabrication and could be performed as a sensor for analysis of AAP in the complex matrix samples. The Co_3O_4 nanoflakes based AAP sensor showed excellent performance towards the electrooxidation of AAP in 0.1 M PBS. The high reproducibility, low detection limit and good selectivity of the sensor make the Co_3O_4 nanoflakes a better candidate for AAP detection in the biological samples and commercial pharmaceutical preparations.

DECLARATION OF COMPETING INTEREST

The authors declare that they have no known competing financial interests or personal relationships that could have appeared to influence the work reported in this paper.

ACKNOWLEDGEMENTS

Anhui Provincial Natural Science Foundation (No. 1908085 MB 52) supported this work.

References

1. I. Cazacu, G. Miremont-Salame, C. Mogosan, A. Fourrier-Reglat, F. Loghin and F. Haramburu, *Eur. J. Clin. Pharmacol.*, 71 (2015) 625−629.
2. S. Hiendrawan, B. Veriansyah, E. Widjojokusumo, S.N. Soewandhi, S. Wikarsa and R.R. Tjandrawinata, *Int. J. Pharm.,* 497 (2016) 106−113.
3. A. Raskovic, S. Gigov, I. Capo, M. Paut Kusturica, B. Milijasevic, S. Kojic-Damjanov and N. Martic, *Eur. J. Drug Metab. Pharmacokinet*., 42 (2017) 849−856.
4. M.E. Bosch, A.J.R. Sanchez, F.S. Rojas and C.B. Ojeda, *J. Pharm. Biomed. Anal*., 42 (2006) 291−321.
5. J.C. McCrae, E.E. Morrison, I.M. MacIntyre, J.W. Dear and D.J. Webb, *Br. J. Clin. Pharmacol.*, 84 (2018) 2218−2230.
6. E. Chiam, L. Weinberg, M. Bailey, L. McNicol and R. Bellomo, *Br. J. Clin. Pharmacol*., 81 (2016) 605−612.
7. S. Abbasi, S. A. Haeri and S. Sajjadifar, *Microchem. J*., 146 (2019) 106−114.
8. X. Zhang, R. Li, W. Hu, J. Zeng, X. Jiang and L. Wang, *Biomed. Chromatogr*., 32 (2018) e4331.
9. M. Kyriakides, L. Maitre, B.D. Stamper, I. Mohar, T.J. Kavanagh, J. Foster, I.D. Wilson, E. Holmes, S.D. Nelson and M. Coen, *Arch. Toxicol.*, 90 (2016) 3073−3085.
10. X. Liu, W. Na, H. Liu and X. Su, *Biosens. Bioelectron*., 98 (2017) 222−226.
11. L. Lahuerta-Zamora and A.M. Mellado-Romero, *Anal. Bioanal. Chem.*, 409 (2017) 3891−3898.
12. Q. Chu, L. Jiang, X. Tian and J. Ye, *Anal. Chim. Acta*, 606 (2008) 246–251.
13. M.A. Mallah, S.T.H. Sherazi, M.I. Bhanger, S.A. Mahesar and M.A. Bajeer, *Spectrochim. Acta*, *Part A*, 141 (2015) 64−70.
14. S. Kesavan and S. Abraham John, *J. Electroanal. Chem.*, 760 (2016) 6−14.
15. S. Lotfi and H. Veisi, *Mater. Sci. Eng. C*, 105 (2019) 110112.
16. N.B. Almandil, M. Ibrahim, H. Ibrahim, A.N. Kawde, I. Shehatta and S. Akhtar, *RSC Adv.*, 9 (2019) 15986−15996.
17. S.J. Saleem and M. Guler, *Electroanalysis*, 31 (2019) 2187−2198.
18. S.K. Ponnaiah, P. Prakash and B. Vellaichamy, *Ultrason. Sonochem*., 44 (2018) 196−203.
19. M. Taleb, R. Ivanov, S. Bereznev, S.H. Kazemi and I. Hussainova, *J. Electroanal. Chem.*, 823 (2018) 184−192.
20. A. Martin Santos, A. Wong, A. Araujo Almeida and O. Fatibello-Filho, *Talanta*, 174 (2017) 610−618.
21. V.R. Shinde, S.B. Mahadik, T.P. Gujar and C.D. Lokhande, *Appl. Surf. Sci.*, 252 (2006) 7487–7492.
22. F. Sÿvegl, B. Orel, I. Grabec-Sÿvegl and V. Kauc, *Electrochim. Acta*, 45 (2000) 4359–4371.
23. D. Barreca, C. Massign, S. Daolio, M. Fabrizio, C. Piccirillo, L. Armelao and E. Tondello, *Chem. Mater.*, 13 (2001) 588–593.
24. M.T. Niu, Y.S. Wang, Y. Cheng, G.X. Chen and L.F. Cui, *Mater. Lett.*, 63 (2009) 837–839.
25. D.X. Zhang, X.M. Li, X.G. Guo and C. Lai, *Mater. Lett*., 126 (2014) 211–213.
26. D.E. Zhang, F. Li , A.M. Chen, Q. Xie, M.Y. Wang, X.B. Zhang, S.Z. Li, J.Y. Gong, G.Q. Han, A.L. Ying and Z.W. Tong, *Solid State Sci.*, 13 (2011) 1221–1225.
27. S. Akhter, W.J. Basirun, Y. Alias, M.R. Johan, S. Bagheri, M. Shalauddin, M. Ladan and N.S. Anuar, *Anal. Biochem*., 551 (2018) 29−36.
28. A.M. Campos, P.A. Raymundo-Pereira, C.D. Mendonca, M.L Calegaro, S.A.S. Machado and O.N. Oliveira, *ACS Appl. Nano Mater.*, 1 (2018) 654−661.
29. T.Y. Huang, C.W. Kung, H.Y. Wei, K.M. Boopathi, C.W. Chu and K.C. Ho, *J. Mater. Chem. A*, 2 (2014) 7229−7237.
30. N.S.K. Gowthaman, H.N. Lim and S. Shankar, *ACS Appl. Nano Mater*., 3 (2020) 1213−1222.
31. C. Sauerbrey, *Z. Phys.*, 2 (1959), 206–222.
32. Y. Ding, Y. Wang, L. Su, M. Bellagamba, H. Zhang and Y. Lei, *Biosens. Bioelectron.*, 26 (2010)

542–548.
33. M. Jafarian, M.G. Mahjani, H. Heli, F. Gobal. H. Khajehsharifi and M.H. Hamedi, *Electrochim. Acta*, 48 (2003) 3423–3429.
34. N.S.K. Gowthaman, B. Sinduja, S. Shankar and S.A. John, *Sustain. Energ. Fuels*, 2 (2018) 1588−1599.
35. N.S.K. Gowthaman, P. Arul, J.J. Shim and S.A John, *Appl. Surf. Sci.*, 495 (2019) 143550.
36. I.G. Casclla, *J. Electroanal. Chem.*, 520 (2002) 119–125.
37. Y.E. Bouabi, A. Farahi, N. Labjar, S.E. Hajjaji, M. Bakasse and M.A.E. Mhammedi, *Mater. Sci. Eng. C*, 58 (2016) 70−77.